An Efficient Regenerative Braking System Based on Battery/Supercapacitor for Electric, Hybrid, and Plug-In Hybrid Electric Vehicles With BLDC Motor

Farshid Naseri, *Student Member, IEEE*, Ebrahim Farjah, *Member, IEEE*, and Teymoor Ghanbari

***Abstract*—Complementary features of batteries and supercapacitors can be effectively used in a hybrid energy storage system (HESS). The utilization of the HESS in electric vehicles (EVs) offers many advantages, such as efficient regenerative braking, battery safety, and improved vehicle acceleration. In this paper, a new regenerative braking system (RBS) is proposed for EVs with HESS and driven by brushless DC (BLDC) motor. During regenerative braking, the BLDC acts as a generator. Hence, by using an appropriate switching algorithm, the dc-link voltage is boosted and the energy is transferred to the supercapacitor or the battery through the inverter. The harvested energy can be utilized to improve the vehicle acceleration and/or keep the battery pack from deep discharging while driving uphill. To provide a reliable and smooth brake, braking force distribution is realized through an artificial neural network. Simultaneously, the braking current is adjusted by a PI controller for constant torque braking. To evaluate the performance of the proposed RBS, different simulations and experiments are carried out. The results confirm high capability of the proposed RBS.**

***Index Terms*—Artificial neural network (ANN), brushless DC (BLDC) motor, electric vehicle (EV), hybrid energy storage system (HESS), regenerative braking system (RBS), supercapacitor.**

I. Introduction

ELECTRIC vehicles (EV) are gaining increasing attention for having unique features such as low emission, high efficiency, quiet operation, etc. [1]–[3]. Chemical batteries have long been used as the main energy storage system (ESS) in many industrial applications. They are currently the dominant technology in the electric car industry. However, the chemical batteries have many shortcomings, such as limited cycle-life, limited power density as well as high cost [1]–[4]. Electric double layer capacitors, known as supercapacitors, are high capacitance capacitors that offer many outstanding features such as high power density, long life-cycle, and wide operating temperature range. A qualitative comparison between the lead-acid batteries and supercapacitors is shown in Fig. 1 by the radar chart [4]. As shown, although the supercapacitor offers better performance in most of the terms, it cannot be used as the main ESS since its energy density is relatively low. Likewise, since the technology of the supercapacitors is recently developed, they are not as reliable as the conventional batteries. Complementary features of batteries and supercapacitors can be utilized in a hybrid energy storage system (HESS) [4]–[24]. The application of HESS has many advantages that are listed as follows.

1) High power density of the supercapacitor can be used to effectively harness the kinetic energy of the vehicle during braking.
2) Supercapacitor can assist the battery pack in peak power demands, which not only prolongs the battery life time but also improves the vehicle acceleration.
3) Since the braking energy could be effectively saved, the drive range of the vehicle can be considerably increased [25]–[31].

During the past decade, many efforts have been made to use the supercapacitors in EVs to overcome the deficiencies of the batteries. Extreme Hybrid is the first commercialized plug-in hybrid electric vehicle (PHEV) technology that actively combines batteries and supercapacitors in a HESS, developed by AFS Trinity Power Corporation [32]. Different configurations for HESS are described in [2], [21]. One of the most studied and researched HESSs is the supercapacitor/battery topology [6], where the battery pack is directly connected to the DC-bus. A bidirectional DC/DC converter is utilized to control the power flow between the battery and supercapacitor. Since two individual ESSs and an additional power converter are required for HESSs, they are generally not cost efficient. Moreover, the bidirectional converter is necessary to match the power level of the supercapacitor module to utilize the capabilities of the supercapacitor effectively [21]. Therefore, the overall system cost would be high.

In this paper, a novel structure for desirable interaction of the battery and supercapacitor is proposed. The presented HESS is composed of a supercapacitor module, battery pack, buck converter, and a diode. Different operation modes of the proposed HESS are discussed in detail. Moreover, for the proposed HESS, a new RBS is developed. During the braking process, using an appropriate switching algorithm for the inverter, the dc-link voltage is boosted. Hence, the diode will be forward biased and the braking energy is directly harvested by the supercapacitor module without employing an additional

Manuscript received February 15, 2016; revised June 16, 2016; accepted September 3, 2016. Date of publication September 20, 2016; date of current version May 12, 2017. The reviewer of this paper is S. Anwar.

F. Naseri and E. Farjah are with the School of Electrical and Computer Engineering, Shiraz University, Shiraz 71847-64175, Iran (e-mail: f.naseri@shirazu.ac.ir; farjah@shirazu.ac.ir).

T. Ghanbari is with the School of Advanced Technologies, Shiraz University, Shiraz 71847-64175, Iran (e-mail: teymoor_ghanbari@yahoo.com).

Color versions of one or more of the figures in this paper are available online at http://ieeexplore.ieee.org.

Digital Object Identifier 10.1109/TVT.2016.2611655

0018-9545 © 2016 IEEE. Personal use is permitted, but republication/redistribution requires IEEE permission.
See http://www.ieee.org/publications_standards/publications/rights/index.html for more information.

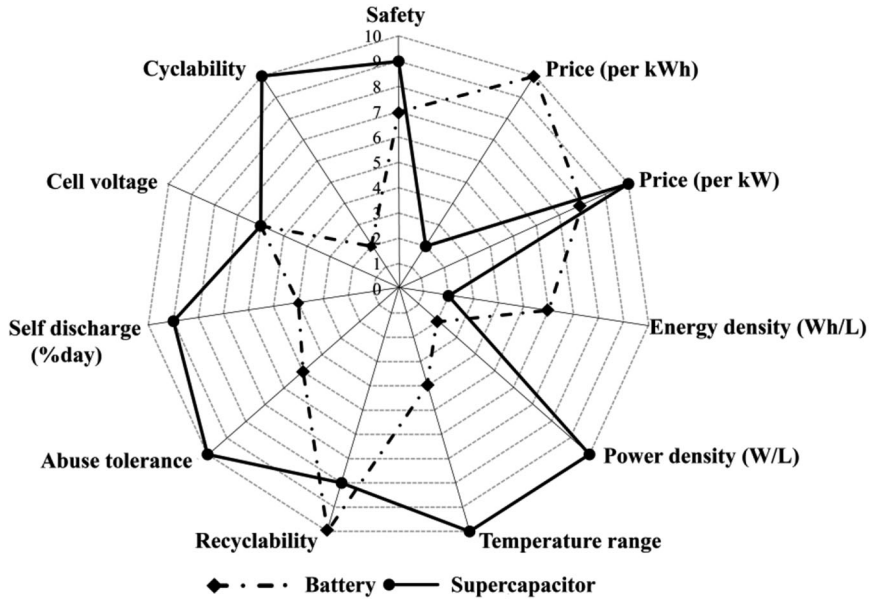

Fig. 1. Qualitative comparison of the Lead–Acid battery and supercapacitor.

power converter. The dc-link voltage is adjusted through variation of the duty-cycle of the pulse width modulation (PWM) in the inverter. Hence, when the supercapacitor is almost charged, regenerative braking can be realized by means of the battery pack. In the proposed method, the regenerative braking efficiency is improved due to the elimination of the utilized converters for this purpose [25]. Moreover, an artificial neural network (ANN) is utilized to achieve braking force distribution. Meanwhile, a PI controller is used to adjust the braking current in such a way that the braking torque is kept constant. A qualitative comparison of different HESS designs in EV applications is provided in Table I. The rest of the paper is organized as follows.

In Section II, the topology and the operation modes of the proposed HESS are discussed. In Section III, the detailed analysis of the developed RBS is presented. Section IV presents the simulation and experimental results to demonstrate the feasibility and superiorities of the proposed HESS. Finally, the main results are concluded in Section V.

II. Structure and Operation Modes of the Proposed HESS

The structure of the proposed HESS is shown in Fig. 2. In the proposed topology $V_{\rm Batt} = V_{\rm DC} \leq V_{\rm sc}$, $V_{\rm Batt}$ refers to voltage of the battery pack, $V_{\rm DC}$ refers to voltage of the dc-link, and $V_{\rm SC}$ is voltage of the supercapacitor module. In other words, a lower voltage battery pack is directly connected to the dc-link and, hence the dc-link voltage is relatively constant. A higher voltage supercapacitor module is connected to the battery pack through a unidirectional DC/DC buck converter. Meanwhile, the battery pack is paralleled with the supercapacitor module through a diode, as shown in Fig. 2. The HESS is utilized to supply the BLDC motor via the three-phase inverter. In normal conditions, the battery is solely used to supply the BLDC motor. In peak power demand occasions, such as vehicle acceleration or

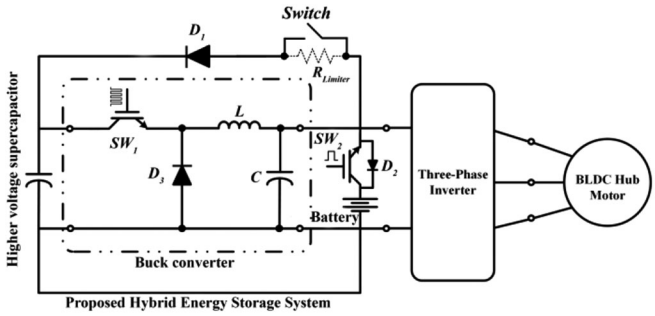

Fig. 2. Structure of the proposed HESS.

driving uphill, the supercapacitor module assists the battery pack through the buck converter. The power converter is controlled to keep voltage of the supercapacitor module higher than the battery pack voltage, and hence the diode is usually reverse biased. During the vehicle braking, the BLDC machine acts as a generator. Consequently, by utilizing the MOSFETs in the three-phase inverter as well as the motor inductances and adopting a suitable switching pattern, a boost chopper can be formed. Accordingly, during the regenerative braking process, the dc-link voltage is boosted and the diode is forward biased. Hence, the braking energy can be efficiently harvested by the supercapacitor module.

It should be noted that an ESS with higher voltage capacity leads to some balancing challenges since several individual cells are required to be utilized. Balancing circuits for the supercapacitor modules, however, are often less expensive and easier to implement in comparison with the batteries. Moreover, the supercapacitor state of charge (SOC) can be easily measured since it is proportional to the supercapacitor voltage. Therefore, utilizing a higher voltage supercapacitor module has many advantages from the implementation aspect.

Due to the self-discharge of the supercapacitor, voltage across terminals of the supercapacitor module will decay if the HESS

TABLE I
QUALITATIVE COMPARISON OF DIFFERENT HYBRID ENERGY STORAGE SYSTEM DESIGNS IN EV APPLICATIONS

HESS	Overall cost	Control complexity	Performance	
			Advantage	Disadvantage
Passive [5]	Very Low	Very Low	• It has a simple structure. • It is very cost-effective. • It does not require a control circuit.	• Supercapacitor stored energy is not effectively utilized. • There is no overcurrent protection mechanism for the battery. • Voltage strategy of the battery and supercapacitor must be necessarily matched.
Supercapacitor/Battery [6]	Medium	Medium	• The stored energy of the supercapacitor can be effectively used. • Since the battery is connected to the DC-link, the voltage of DC-link is relatively constant, and hence complicated voltage control loops may be eliminated.	• A bidirectional DC/DC converter with high power rating is required. • Due to the power dissipation of bidirectional DC/DC converter, the efficiency of regenerative braking is decreased.
Battery/Supercapacitor [7]-[8]	Medium	High	• The supercapacitor acts like a Low Pass Filter (LPF) and directly handles the load transients. • Rated voltage of the battery can be lowered.	• The ratings of the switches in the motor drive are increased.
Cascaded Converters [9]-[10]	High	High	• The stored energy of the supercapacitor can be effectively used.	• Two bidirectional DC/DC converters with high power ratings are required which increases the overall cost of the system. • Efficiency is low due to the existence of two DC/DC converters. • Due to the power dissipation of bidirectional DC/DC converter, the efficiency of regenerative braking is decreased.
Multiple Parallel-Connected Converters [11]-[12]-[13]-[32]	Very High	High	• The system has better flexibility and functionality. • The efficiency of the system is high. • The reliability of the system is high.	• It requires two DC/DC converters with high power rating. • Due to the power dissipation of bidirectional DC/DC converter, the efficiency of regenerative braking is decreased.
Multiple Dual-Active-Bridge Converters Topology [14]	Very High	High	• Battery and supercapacitor are electrically isolated by magnetic coupling of transformer.	• Number of semiconductor switches is high which increases the cost. • It does not provide bidirectional power transfer capability for regenerative braking. • The reliability of the system is decreased due to large number of components.
Dual-Source Bidirectional Converters Topology [15]-[16]	High	Very High	• The system has better flexibility and functionality. • The efficiency of the system is high. • The reliability of the system is high.	• Due to the power dissipation of bidirectional DC/DC converter, the efficiency of regenerative braking is decreased. • It requires complicated control design.
Multiple-Input Converter Topology [17]-[18]-[19]-[20]	High	Very High	• Only one inductor is required. • Overall weight and volume of the converter is reduced.	• It requires complicated control design.
Multiple Modes Single-Converter Topology [21]	Medium	Medium	• The supercapacitor acts like a Low Pass Filter (LPF) and directly handles the load transients. • Rated voltage of the battery can be lowered.	• Due to the voltage fluctuations of the DC-link, the ratings of the switches in the inverter must be increased. • Rated voltage of the supercapacitor is always higher than the battery, which puts limitations on system design.
Proposed HESS	Low	High	• Due to the elimination of power electronics interfaces, the efficiency of the regenerative braking is increased. • Since the battery is connected to the DC-link, the voltage of DC-link is relatively constant and complicated voltage control loops may be eliminated. • It needs an unidirectional DC/DC converter.	• Since the supercapacitor can only be discharged to the extent that its voltage remains larger than the battery, the supercapacitor stored energy cannot be fully utilized. • Rated voltage of the supercapacitor is always higher than the battery, which puts limitations on system design.

is not recharged for a while. Under this circumstance, when the system starts up (SW_2 is turned ON), the regenerative diode D_1 is forward biased and an inrush current is drawn from the battery pack to the supercapacitor module. Hence, the battery pack and diode D_1 can be damaged. To rectify the foregoing problem, a limiter resistance is inserted in series with the regenerative diode to restrain the inrush current drawn by the supercapacitor module in such a condition. When the supercapacitor module is charged to a level of the battery voltage, the limiter resistance is bypassed using a mechanical switch. The limiter resistance can also be utilized for protection of the battery during normal operation, e.g., when diode D_1 is short circuited.

Depending on the amplitude and direction of the motor demanded power P_{motor}, operation of the proposed HESS can be categorized into four different modes, which are discussed in the following.

A. Vehicle Normal Mode

Whenever the motor power P_{motor} is equal to or less than the battery rated power $P_{\text{Batt,rated}}$, the vehicle normal mode is activated. The energy flow in the normal mode is shown in Fig. 3(a). In this mode, since the supercapacitor voltage is higher than the battery voltage, D_1 is reverse biased. Moreover, the buck converter is turned OFF and the supercapacitor module is idle. The battery pack solely supplies the BLDC motor in this condition.

B. Vehicle Acceleration Mode

During the vehicle acceleration, driving uphill and vehicle top speeds, the motor power P_{motor} exceeds the battery rated power $P_{\text{Batt,rated}}$, which is referred to here as vehicle acceleration mode. Under such circumstance, the battery pack could undergo frequent deep discharge cycles and the performance of the vehicle could also be degraded. Under these conditions, if the supercapacitor voltage is greater than the minimum threshold ($V_{\text{sc}} \geq V_{\text{SC,min}}$), the supercapacitor assists the battery pack through the DC–DC converter. Fig. 3(b) shows the energy flow in this mode. If V_{SC} drops below V_{Battery} in these conditions, the battery pack could unwantedly charge the supercapacitor module, which increases the stresses in the battery pack. Therefore, supercapacitor assists the battery pack only until V_{SC} is higher than V_{Battery},which is dictated by the control system. Under these conditions, D_1 is always reverse biased and the energies of both the supercapacitor module and the battery pack are supplying the BLDC motor.

C. Regenerative Braking With Supercapacitor

Due to the voltage strategy of the supercapacitor and battery, D_1 is usually reverse biased under normal conditions. In the regenerative braking events, the dc-link voltage must be boosted so that D_1 is forward biased and the braking energy could be harvested by the supercapacitor module. This is normally achieved by employing additional boost converters or substituting a bidirectional buck–boost DC/DC converter [25]–[36]. Adding another DC/DC converter not only increases the implementation cost but also decreases the energy transfer efficiency due to the power dissipation of the power electronics interfaces. One cost-effective idea is that by the utilization of the inductances in the three-phase BLDC motor, the bidirectional switches in the three-phase inverter, and employing a suitable switching scheme, the inverter can form a boost circuit. The MOSFETS on the high arms of the H-Bridge are turned OFF and the MOSFETS of the low side are pulse width modulated. The switching algorithms are further discussed in Section III. It should be noted that this mode of operation is activated only if $V_{\text{SC}} \leq V_{\text{SC,max}}$, where $V_{\text{SC,max}}$ is the upper voltage limit of the supercapacitor module that is usually considered for safety of the operation.

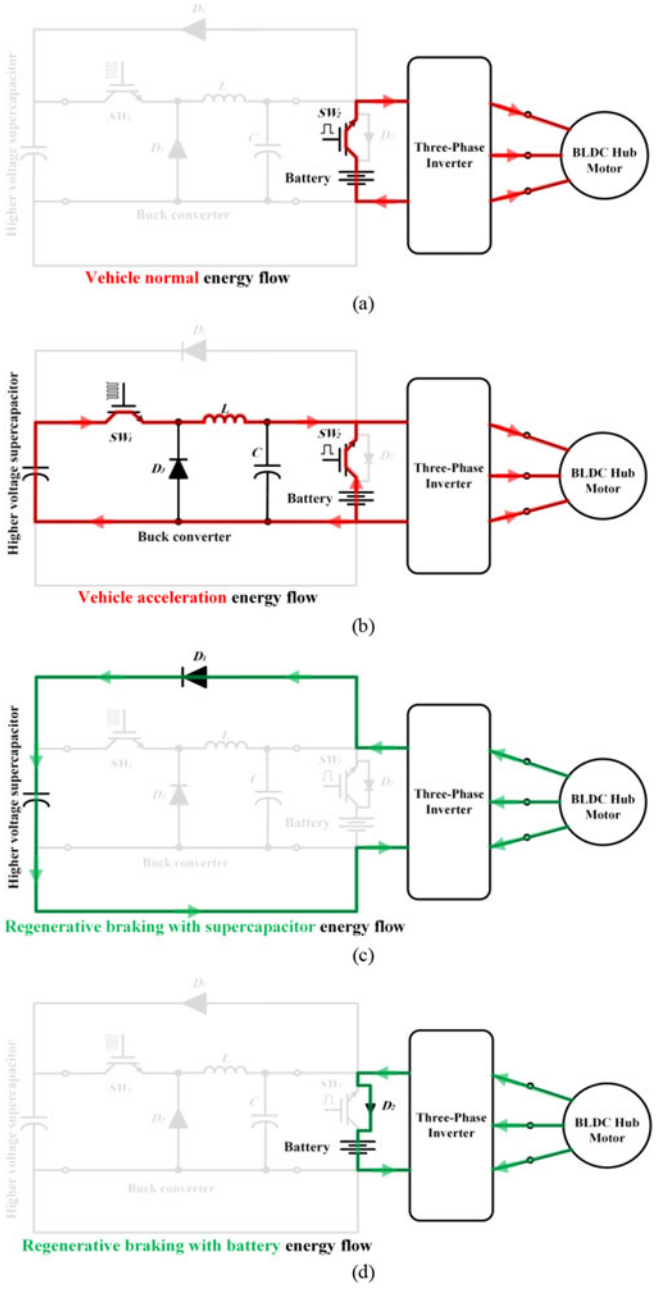

Fig. 3. Energy flow in different operation modes of the proposed HESS. (a) Vehicle normal operation mode of the proposed HESS. (b) Vehicle acceleration mode of the proposed HESS. (c) Vehicle regenerative braking with supercapacitor mode of the proposed HESS. (d) Vehicle regenerative braking with battery mode of the proposed HESS.

D. Regenerative Braking With Battery

If $V_{\text{SC}} \geq V_{\text{SC,max}}$, the braking energy cannot be transferred to the supercapacitor, and hence, regenerative braking is realized by the battery pack. The operation principle of this mode is very similar to that of the previous mode. The dc-link voltage can be boosted in the same manner, and the energy is transferred to the battery pack through D_2.

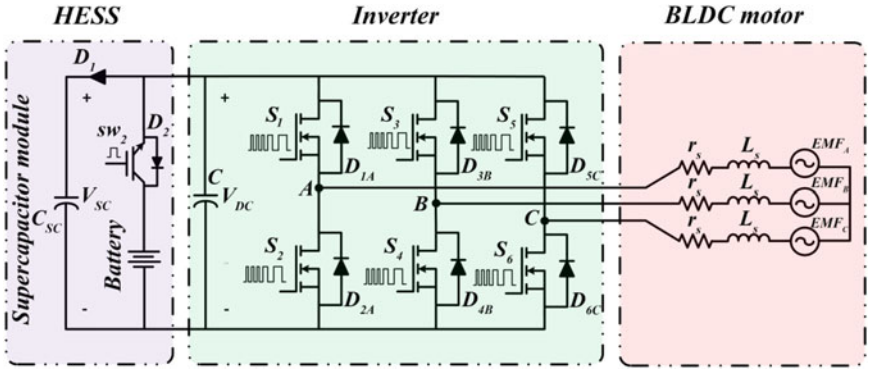

Fig. 4. Equivalent circuit of the voltage source inverter, BLDC motor, and the proposed HESS.

When dc-link voltage is boosted for accomplishment of regenerative braking with the supercapacitor, both D_1 and D_2 are forward biased. Considering dynamics of the braking procedure, battery charging, and supercapacitor charging, it is clear that contribution of the supercapacitor is significantly higher than the battery for capturing the braking energy. In fact, time constant of braking procedure is close to supercapacitor time constant and is much lower than the battery time constant. Moreover, due to lower ESR of the supercapacitor, most of the braking current is absorbed by the supercapacitor. Hence, forward-biasing of D_2 has no considerable impact on the operation of mode C.

III. Analysis of the Proposed RBS

A. Energy Regeneration Using DC/AC Converter

Fig. 4 shows the equivalent circuit of the inverter, the BLDC motor, and the proposed HESS. In Fig. 4, r_s and L_s are the resistance and inductance of the armature, respectively. EMF_A, EMF_B, and EMF_C are the armature back electromotive forces (EMF) of phases *a*, *b*, and *c*, respectively. Since the DC–DC converter is usually idle during braking, it is not shown in Fig. 4. During regenerative braking, the BLDC machine acts as a generator, and the kinetic energy of the vehicle can be stored in the HESS by the reversal of the current flow. To achieve this function, the dc-link voltage needs to be boosted so that D_1 and/or D_2 are/is forward-biased and the energy is transferred to the HESS. The same power circuit of Fig. 4 could be utilized with an appropriate switching template.

In normal conditions, all six switches in the inverter are commutated according to the rotor position, obtained by the hall effect sensors. In the regenerative braking, the switches on the high side of the half bridge are all turned OFF and the low-side MOSFETS are controlled by the PWM with an appropriate switching strategy. The three-phase back EMFs, three-phase armature currents, hall effect signals, and the relevant switching patterns are shown in Fig. 5. In the regenerative braking mode, there are six commutation intervals, and only one of the inverter switches is turned ON and OFF during each interval. The equivalent circuit for one commutation state $(0^\circ - 60^\circ)$ of the regenerative braking with supercapacitor is shown in Fig. 6. Suppose S_2 is ON for a time interval t_{on}. The current ramps up linearly in $2L_S$ to a peak value $I_P = \frac{V_{\mathrm{EMF}} \times t_{\mathrm{on}}}{L_S}$. Therefore, the

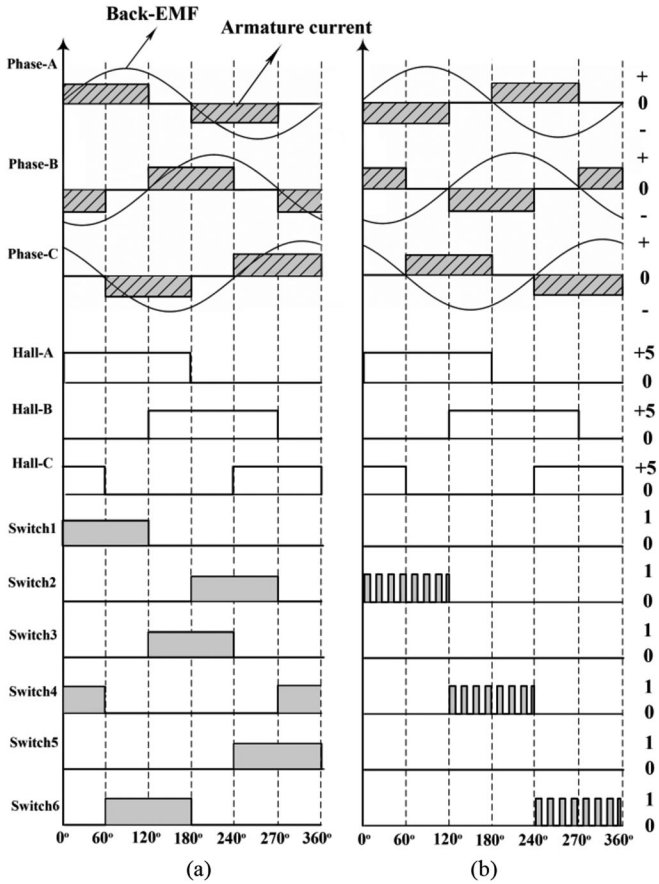

Fig. 5. Waveforms of the back EMFs, armature currents, hall effect sensors, and the switching template. (a) Waveforms in the normal condition. (b) Waveforms in the regenerative braking mode.

amount of the stored energy in the inductor can be represented as follows:

$$E = \frac{1}{2}(2L_S)I_P^2 = L_S I_P^2 \tag{1}$$

where *E* is in Joules, L_S is in Henries, and I_P is in Amperes.

During S_2 is ON, the output is solely supplied from *C*, which is selected large enough to supply the output for time interval t_{on} with a minimum voltage drop. When S_2 is turned OFF, D_{1A} is forward biased and both the energy from back EMFs

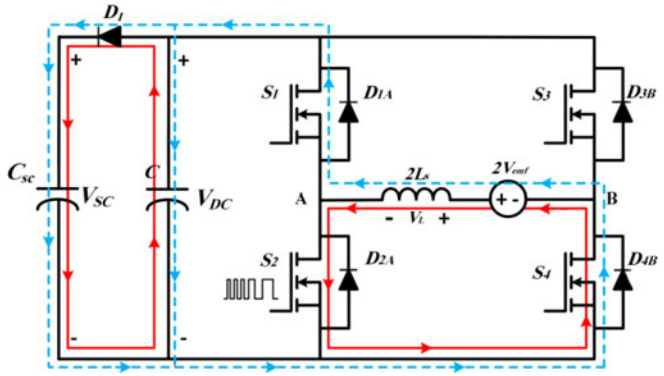

Fig. 6. Operational behavior of the inverter circuit under regeneration condition at each subinterval.

and the stored energy in the inductor are utilized to supply the supercapacitor. Under this condition, the output voltage is regulated by controlling the S_2 ON time in a negative feedback loop by the PI controller. If all the energies of (1) could be transferred to the output during each period T (assuming 100% conversion efficiency), the transferred power to the load from $2L_S$ is as follows:

$$P_{\text{inductor}} = \frac{\frac{1}{2} \times 2L_S \times I_P^2}{T} = \frac{L_S \times I_P^2}{T}. \tag{2}$$

Additionally, an amount of power P_{DC} is transferred to the output from $2V_{\text{EMF}}$, which can be represented as follows:

$$P_{\text{dc}} = 2V_{\text{EMF}} \times \frac{I_P}{2} \times \frac{T_r}{T} \tag{3}$$

where T_r is the time interval at which the current in the inductor ramps down to zero. Hence, the overall power delivered to the load can be calculated as follows:

$$P_{\text{total}} = P_{\text{inductor}} + P_{\text{dc}} = \frac{L_S \times I_P^2}{T} + 2V_{\text{EMF}} \times \frac{I_P}{2} \times \frac{T_r}{T}. \tag{4}$$

Substituting $I_P = \frac{V_{\text{EMF}} \times t_{\text{on}}}{L_S}$, one can rewrite

$$P_{\text{total}} = \frac{V_{\text{EMF}}^2 \times t_{\text{on}}}{T \times L_S} \times (t_{\text{on}} + t_r). \tag{5}$$

It is assumed that the circuit works in the discontinuous mode, and hence $t_{\text{on}} + t_r = mT$, where m is a fraction less than 1. Equation (5) can be rewritten as follows:

$$P_{\text{total}} = \frac{V_{\text{EMF}}^2 \times t_{\text{on}}}{T \times L_S} \times m \times T. \tag{6}$$

For an output voltage of V_{dc}, one can write

$$P_{\text{total}} = \frac{V_{\text{EMF}}^2 \times t_{\text{on}}}{T \times L_S} \times m \times T = \frac{V_{\text{dc}}^2}{R} \tag{7}$$

where R is the output resistance. With some manipulations, the conversion ratio is obtained as follows:

$$\frac{V_{\text{dc}}}{V_{\text{EMF}}} = \sqrt{\frac{R \times t_{\text{on}} \times m}{L_S}}. \tag{8}$$

The conversion ratio is plotted versus the duty cycle as shown in Fig. 7.

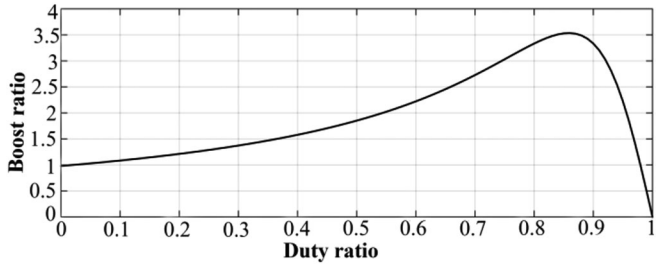

Fig. 7. Boost capability of the dc-link voltage in the proposed RBS.

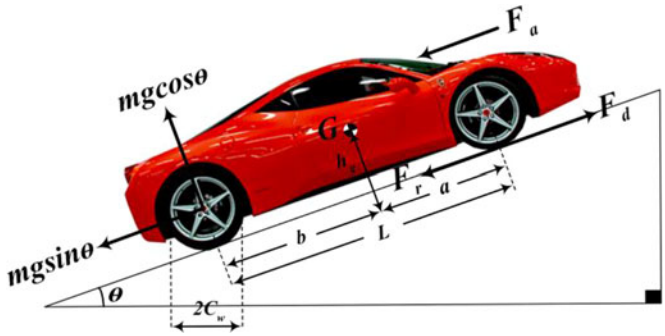

Fig. 8. Forces acting against the EV during driving and two-axle braking dynamics of the EV.

B. Road Load and Traction Forces of the EV

In this paper, a simplified model of the road vehicle kinematics is used for estimation of the dynamic tractive requirements of the EV powertrain. This model represents the driving forces of the vehicle, as shown in Fig. 8. Generally, these forces can be categorized into four main components which are introduced below.

1) Rolling Resistance Losses: This is the required force to overcome the friction between the tires and the road, which is known as rolling resistance and can be represented by

$$F_r = K_r mg \cos\theta \tag{9}$$

where K_r is the coefficient of the rolling resistance, m is the vehicle and payload overall mass (kg), θ is the slope angle (*degree*), and g is the gravitational constant (m/s^2).

2) Aerodynamics Resistance Losses: Aerodynamics losses result from the friction between the airstream and the body of the vehicle. Aerodynamic resistance can be modeled as follows:

$$F_a = \frac{1}{2}\rho C_d A_f v^2. \tag{10}$$

In (10), ρ is the air density (kg/m^3), C_d is the drag force coefficient, A_f is the frontal area of the vehicle (m^2), and v is the vehicle linear velocity (m/s^2).

3) Road Gradient Force: As shown in Fig. 8, in case of driving on a steep road, the gradient force is created by the gravity that substantially affects the behavior of the vehicle. The road gradient force can be expressed as follows:

$$F_g = mg \sin\theta. \tag{11}$$

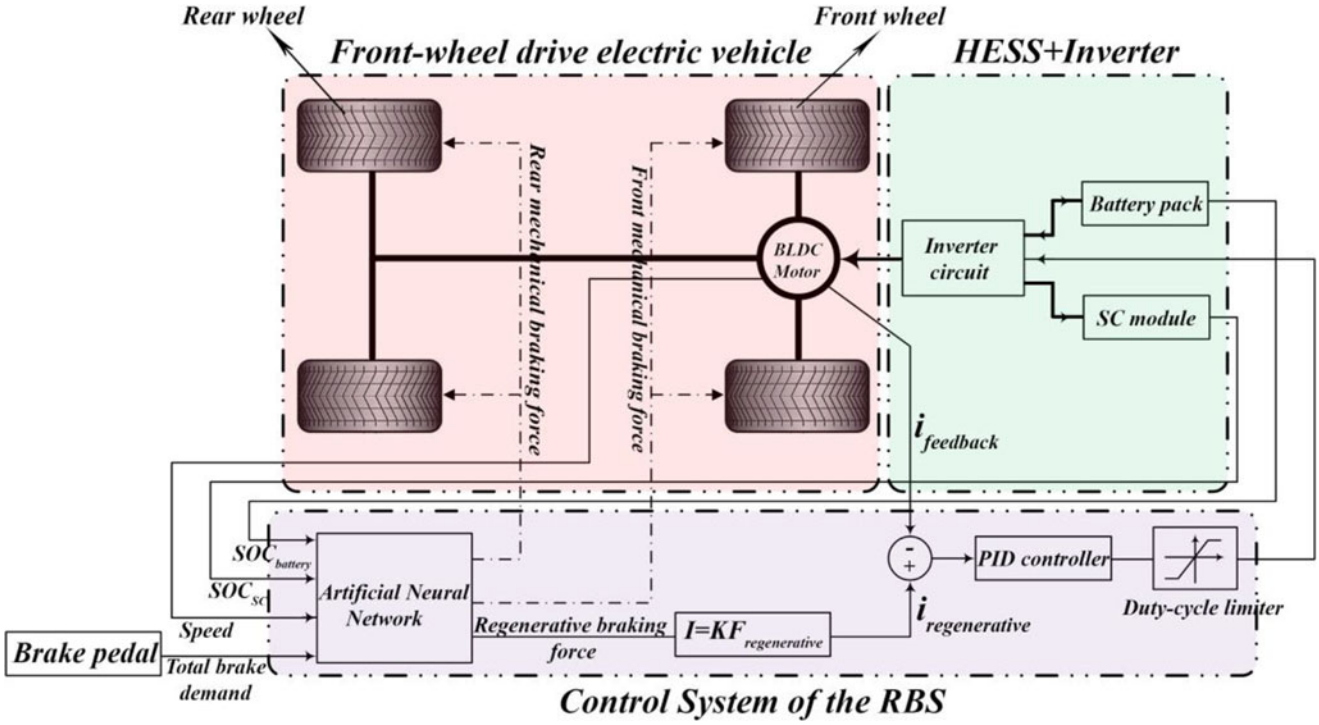

Fig. 9. Structure of the control system of the proposed regenerative braking method.

4) Transient Force: This is the force required to accelerate or retard the vehicle and can be written as $m\frac{dv}{dt}$. Accordingly, the required total force at the wheels of the vehicle can be derived as follows:

$$F_d = F_r + F_g + F_a + m\frac{dv}{dt}. \tag{12}$$

Substituting (9)–(11) in (12) yields

$$m\frac{dv}{dt} = F_d - K_r mg\cos\theta - \frac{1}{2}\rho C_d A_f v^2 - mg\sin\theta. \tag{13}$$

In (13), F_d is the supplied force by the vehicle engine to drive the car. Equation (13) can be utilized to obtain the required braking torque to stop the vehicle at a predetermined distance specified by the drive cycle.

C. Control Strategy of the Proposed RBS

Structure of the control strategy system is shown in Fig. 9. The braking force distribution, the ANN, and the PI controller are the main sections of the proposed structure, which are discussed in different sections as follows.

1) Braking Force Distribution: During braking, kinetic energy of the EV will be transferred to the energy storage device. On some braking occasions, the HESS will reach its maximum capacity, and it cannot accept further charge from the BLDC machine, which limits the regenerative capability. Moreover, the power/torque-handling capability of the electric machine and/or power electronic system are other limiting factors. Therefore, involvement of frictional braking is critical for accomplishing the braking objective. Hence, the total braking force of the car is composed of the rear and front braking forces

$$F_{\text{car}} = F_{\text{front}} + F_{\text{rear}} \tag{14}$$

where F_{front} is composed of mechanical and regenerative forces, and F_{rear} is pure mechanical force. These forces can be written as follows:

$$F_{\text{front}} = \phi.\frac{m.g.(b + z.h_g)}{L} \tag{15}$$

$$F_{\text{rear}} = \phi.\frac{m.g.(a - z.h_g)}{L}. \tag{16}$$

In (15) and (16), φ is the adhesion coefficient, *m* is the vehicle load, *g* is the gravitational constant, *b* is the centroid of the vehicle to the rear axle centerline distance, *a* is the centroid of the vehicle to the front axle centerline distance, h_g is the height of the centroid of the EV, and *L* is the distance from the rear axle to the front axle of the EV ($L = a + b$). Moreover, *z* is defined as $z = \frac{\alpha_{\text{car}}}{g}$, where α_{car} is the acceleration of the vehicle.

Adding (15) to (16) yields

$$F_{\text{car}} = F_{\text{front}} + F_{\text{rear}} = \phi.m.g. \tag{17}$$

According to the ideal braking force distribution curve [27], the maximum braking force that can make the rear and front wheels lock simultaneously for every possible adhesion coefficient can be obtained using

$$F_{\text{rear}} = \frac{1}{2}\left[\frac{m.g}{h_g}\sqrt{b^2 + \frac{4h_g L}{mg}F_{\text{front}}} - \left(\frac{mgb}{h_g} + 2F_{\text{front}}\right)\right]. \tag{18}$$

Solving (17) and (18) yields the required braking force at the rear and front wheels of the vehicle. The braking force

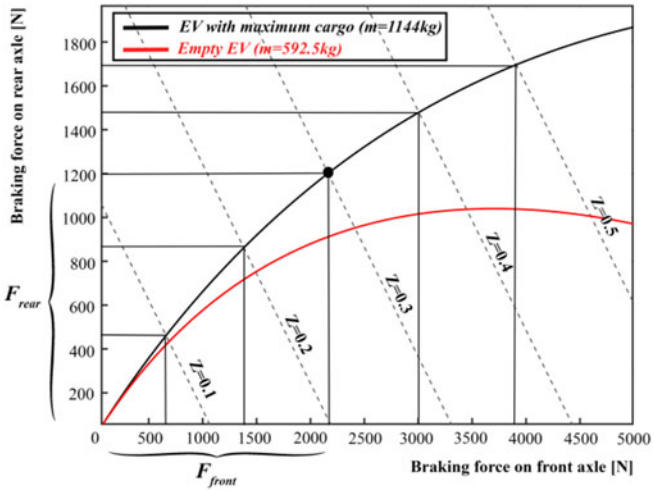

Fig. 10. Braking force distribution between the front and rear wheels for the studied EV.

TABLE II
PARAMETERS OF THE EV AND THE ROAD CONDITIONS

Parameter	Definition	Value
ρ	Air density	1.2 kg/m^3
G	Gravitational constant	9.8 m/s^2
θ	Slope angle	0°
A_f	Frontal area of the EV	2 m^2
C_w	Radius of the wheel	0.335 m
h_g	height of the centroid of the EV	0.5 m
M	EV mass (with cargo)	1144 kg
L	distance from rear axle to the front axle	2.6 m
A	centroid of the vehicle to the front axle centerline	1.2 m
B	centroid of the vehicle to the rear axle centerline	1.4 m
K_r	coefficient of the rolling resistance	0.009

distribution curve for the EV studied in this paper is shown in Fig. 10. It can be seen that the weight of the EV considerably affects the dynamic behavior of braking. In this paper, the weight of the EV, including cargo and HESS, is 1144 kg. Other parameters of the EV are listed in Table II.

2) ANN Controller: The concept of the proposed control strategy is illustrated in Fig. 9. When the brake pedal is engaged, in accordance with the depression amount of the pedal, the required braking force can be obtained through (13). The values of the rear braking force and the front braking force in EVs can be calculated based on the braking force distribution curve, as shown in Fig. 10. Depending on the vehicle conditions, such as velocity and battery SOC, auxiliary controllers like fuzzy logic and lookup table are generally utilized to determine the values of the regenerative braking force and the mechanical braking force for the front wheels (in front-wheel drive EVs). However, in the case of EVs equipped with HESS, the SOCs of both battery and supercapacitor must be taken into account, which leads to implementation complexity. Moreover, in the advanced braking systems, such as electronic braking system and cornering brake control, the braking forces are asymmetrically shared between different wheels of the car to reduce the risk of skidding,

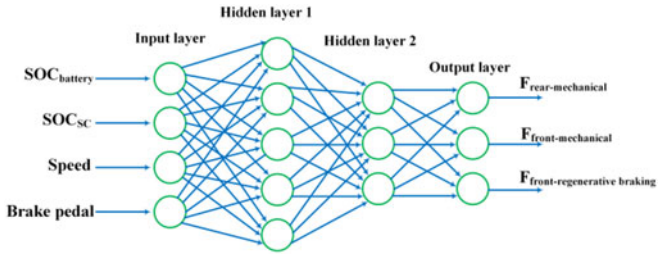

Fig. 11. Structure of the utilized ANN.

spinning, and vehicle instability. The sophisticated dynamics of such systems cannot be easily handled by the aforementioned controllers.

Accordingly, ANN-based controller is proposed to share the required braking force between the rear and front wheels of the EV. ANNs are intelligent computing tools that are constructed from multiple interconnected components, called neurons, which are able to determine the underlying relationship between the input and output patterns [37], [38]. Multilayer perceptron (MLP) and radial basis function are the two well-known structures for the ANNs.

The performance of the ANN essentially depends on the design process. First, all possible cases that the ANN needs to learn must be prepared in a training dataset. Second, the structure of the ANN, including the type, number of the hidden layers, and the number of the neurons in each layer needs to be selected for a given application. The next stage is training the ANN by using the collected datasets. Finally, the trained ANN must be evaluated and validated using some other datasets to check its accuracy in generalization.

Different simulations show that a four-layer feed-forward MLP neural network gives desirable performance for the ANN in this application. The inputs of the MLP network are SOCs of the battery and supercapacitor, the vehicle speed, and the depression of the brake pedal. Two hidden layers with five and three neurons are considered. The outputs of the utilized ANN are the mechanical braking forces of the rear and front wheels and the regenerative braking force of the front wheel. Sigmoid function is selected as the activation function for the neurons in the hidden layers

$$f(u) = \frac{1}{1 + e^{-u/T}}. \tag{19}$$

Likewise, linear transfer function is applied for the neurons in the output layer of the ANN. The structure of the proposed MLP network is shown in Fig. 11. The relationship between the brake strength (pedal depression), the rear braking force, and the front braking force can be calculated straightforwardly using the ideal distribution curve, as shown in Fig. 10. However, the training dataset should also contain sufficient information about the portions of the regenerative braking and the mechanical braking forces for different operating regimes.

To create the training dataset, various simulations are carried out in MATLAB/SIMULINK by applying different values of SOCs for the battery and supercapacitor. The vehicle speed and

the brake strength are established by the training drive cycle. The selection of the drive cycle is very important for simulation of sufficient braking scenarios.

In this paper, INRETS route1 drive cycle is selected. In the selected drive cycle, the EV spends 77.81% of time in braking and/or decelerating conditions. The braking scenarios occur at different EV speeds and different brake strengths. Hence, a rich training dataset can be obtained. The specifications of the training drive cycle can be found in the Appendix. The braking forces are calculated based on three criteria: 1) the vehicle is decelerated or stopped in the specified distance and the time determined by the drive cycle; 2) maximum regeneration is achieved; and 3) SOCs of battery and supercapacitor remain within the safe margins. The back propagation technique with Levenberg–Marquardt method is used to train the ANN. One explicit criterion to evaluate the performance of the ANNs is the normalized root mean square error (NRMSE), which is the error between the estimated output and the true output and can be written as follows:

$$\mathrm{NRMSE} = \sqrt{\frac{\sum_n \left[F(n) - F'(n)\right]^2}{\sum_n F'(n)^2}} \tag{20}$$

where $F(n)$ and $F'(n)$ are the estimated and target values of the outputs, respectively, and *n* is the number of data points. In the training stage, 357 different cases are simulated by varying the SOCs. The NRMSE is calculated 0.013 for the third output $F_{\mathrm{front-regenerative-braking}}$. The generalization ability of the ANN should be evaluated using some other braking scenarios that are not used in the training stage. Hence, the ANN is validated using another drive cycle (UG214 Car05) in which 42 different cases are simulated. UG214 Car05 is selected since it has large number of braking scenarios and, thus, the ANN performance can be evaluated effectively. The NRMSE is 0.103 for the same output in this case.

3) PI Controller: After the braking force distribution is accomplished by the ANN, the regenerative braking force of the front wheel is translated to the braking current using

$$I = k \times F_{\mathrm{regenerative}}. \tag{21}$$

Once the current set point is calculated, the PI controller is used to adjust the braking torque by regulating the duty-cycle of the PWM algorithm described in Section II. Hence, the proposed method can achieve constant torque regenerative braking for realizing comfort and security purposes.

The whole procedure of the proposed RBS is illustrated by the flowchart shown in Fig. 12. It should be noted that the computations related to F_{braking}, F_{rear}, and F_{front} shown in Fig. 12 can be easily included in the ANN.

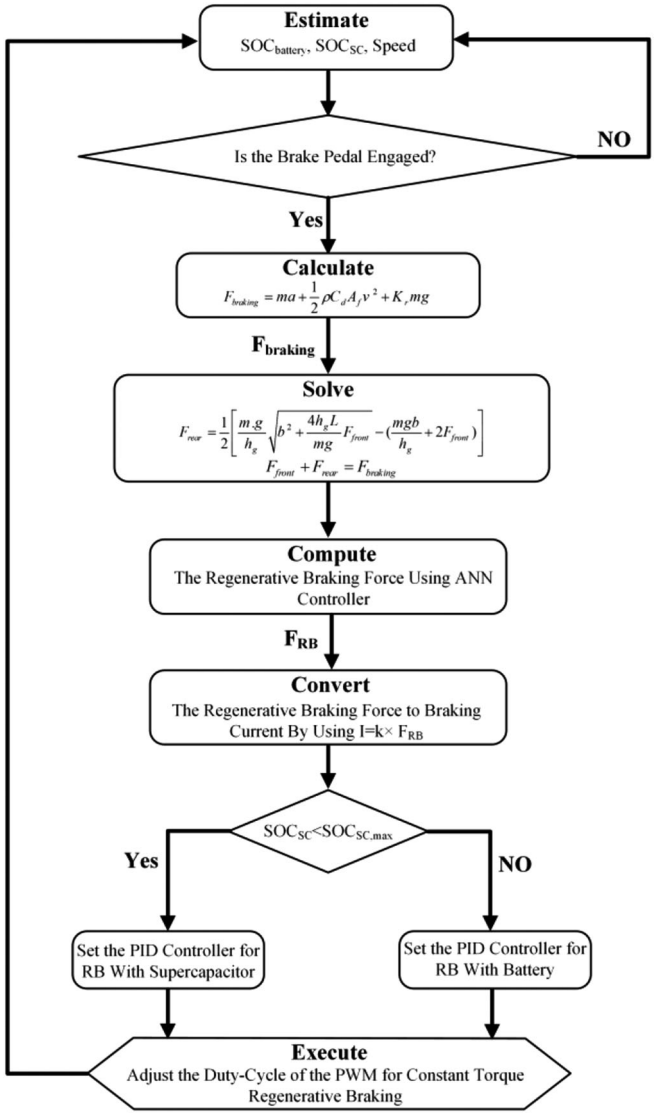

Fig. 12. Flowchart of the proposed regenerative braking system.

D. Description of the EV Components

The EV is modeled in MATLAB/SIMULINK. The schematic of the simulated drivetrain, including mechanical and electrical components, is shown in Fig. 13. The EV model utilized in this paper is VEH_SMCAR from ADVISOR that defines road load parameters for a Saturn SL1. Fig. 8 depicts a two-axle braking dynamics of the EV. In Fig. 8, *G* is the center of gravity of the EV that plays an important role in the braking performance. The EV model weighs about 1144 kg, including the HESS unit and cargo. The conditions of the road and other parameters of the EV are summarized in Table II. The considered electric motor is a BLDC motor with a peak power of 15.8 kW. The battery unit is Lead–Acid and has a nominal voltage of 36 V and weight about 33 kg. The supercapacitor bank is 60 V, 104 F and weight of about 105 kg. The full simulation parameters are presented in Table III.

E. Efficiency Analysis of the Proposed RBS

Generally, the efficiency of the proposed RBS depends on several factors, such as the vehicle speed, SOCs of the battery and supercapacitor, specifications of the drive-cycle, etc. The efficiency can be calculated using

$$\%\eta = \frac{\sum_{i=1}^{n} \Delta E_{\mathrm{SC},i} + \sum_{i=1}^{n} \Delta E_{\mathrm{battery},i}}{\sum_{i=1}^{n} \Delta E_{\mathrm{kinetic}}} \times 100. \tag{22}$$

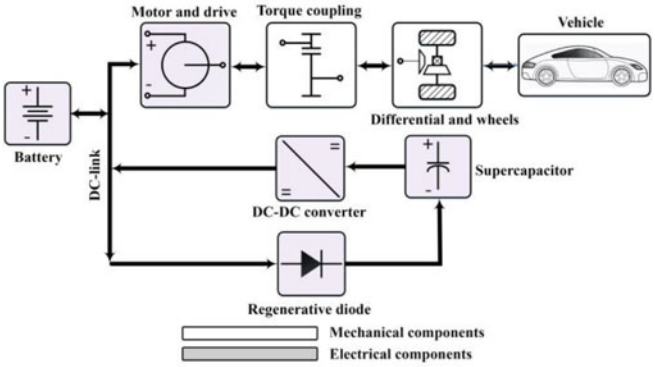

Fig. 13. Simulated drivetrain configuration in MATLAB/SIMULINK.

TABLE III
SIMULATION AND EXPERIMENTAL SPECIFICATIONS

		Parameters	
Simulation	EV Type	Vehicle model	VEH_SMCAR from ADVISOR
		Vehicle overall mass	1144 kg
		Driving type	Front-wheel drive
		Motor	MC_PM8 from ADVISOR
	HESS Specifications	Battery pack	ESS_PB25 12 V 25 Ah (C/10) from ADVISOR/3 packs in series
		Supercapacitor pack	PC2500 MAXWELL 2.5 V 2500 F/24 cells in series and six in parallel
Experimental	Motor specifications	Rated power	5 kW equipped with hall effect sensors
	HESS specifications	Battery pack	12 V 42-Ah Lead–Acid Battery/2 packs in series
		Supercapacitor pack	BMOD0058-E016-B02 MAXWELL 16.2 V 58 F Supercapacitor module/2 modules in series
	Data acquisition system	DS1104 controller board	
	Circuit components	Regenerative diode D_1	DS150-1000L Brown Boveri
		Mosfets	IRFP4127PbF
		Current sensor	CLSM100LA

In (22), *n* is the number of the vehicles decelerating or braking procedures in the drive-cycle. Moreover, $\Delta E_{\rm SC}$, in Joules, is the variation of the energy stored in the supercapacitor module before and after the braking and can be represented as follows:

$$\Delta E_{SC} = \frac{1}{2}C(V_2^2 - V_1^2) \tag{23}$$

where *C* is the capacity of the supercapacitor module in Farads and V_1 and V_2 are the voltages of the supercapacitor module before and after the braking. $\Delta E_{\rm battery}$ (in Joules) is the energy stored in the battery during the braking and can be written as follows:

$$\Delta E_{\rm battery} = \int_{t_1}^{t_2} (V_{\rm battery} i_{\rm battery} - R(t) i_{\rm battery}^2) dt \tag{24}$$

where *R* is the charging resistance of the battery, and $V_{\rm battery}$ and $i_{\rm battery}$ are the voltage and current of the battery pack, respectively. Moreover, t_1 and t_2 are the starting and finishing instants of the braking procedure, respectively. Finally, $\Delta E_{\rm Kinetic}$ is the variation of the kinetic energy (in Joules) of the vehicle, which can be expressed as follows:

$$\Delta E_{\rm Kinetic} = \frac{1}{2}m(v_2^2 - v_1^2) \tag{25}$$

where *m* is the vehicle mass, and v_1 and v_2 are the speed of the vehicle before and after the braking.

TABLE IV
SIMULATION AND EXPERIMENTAL OPERATING LIMITS OF THE BATTERY AND SUPERCAPACITOR

	Limit	
Parameter	Simulation	Experimental
Supercapacitor maximum charge/discharge current	50 A	50 A
Supercapacitor maximum voltage	56.4 V (SOC of 94%)	34 V (SOC of 94%)
Battery maximum charge current	3 A	10 A
Battery maximum discharge current	15 A	20 A
Minimum SOC of battery	30%	30%

IV. SIMULATION AND EXPERIMENTAL RESULTS

The proposed RBS is modeled in MATLAB/SIMULINK. The WVU 5-peak drive cycle is chosen to assess the performance of the RBS. The distance of the drive cycle is 8069.18 meters, with a total travelling time of 900 s. Maximum speed reaches 64.48 km/h, and the EV spends 27.11% of the traveling time in decelerating mode. The whole EV components, including the BLDC motor, battery, supercapacitor, etc., are modeled as lookup tables and efficiency maps based on the empirical measurements obtained from literatures, datasheets, etc. The model uses the desired speeds as inputs and determines the power, speed, and the powertrain torque that meets the speed of the vehicle. The system parameters for the simulations and experiments are tabulated in Table III. Moreover, the operating limits of the battery and supercapacitor are listed in Table IV.

The drive-cycle speed curve is shown in Fig. 14(a). The EV is accelerated from standstill to a constant speed. Then, it is decelerated again to stationary condition. This procedure is repeated four more times at increasing constant speeds. Hence, a realistic driving environment can be simulated in which all the operating modes of the proposed HESS can be activated. Recalling from Section III, substituting the EV parameters (VEH_SMCAR) in (13) yields the driving and braking forces of the vehicle as follows:

$$F_{\rm car} = 1144\frac{dv}{dt} + 0.402v^2 + 101. \tag{26}$$

For example, when the average negative acceleration of the vehicle is 0.373 m/s^2 and the vehicle speed is 9 m/s, the required braking force is -293.15 N, which can be translated to braking torque using

$$T = F_d \times C_w. \tag{27}$$

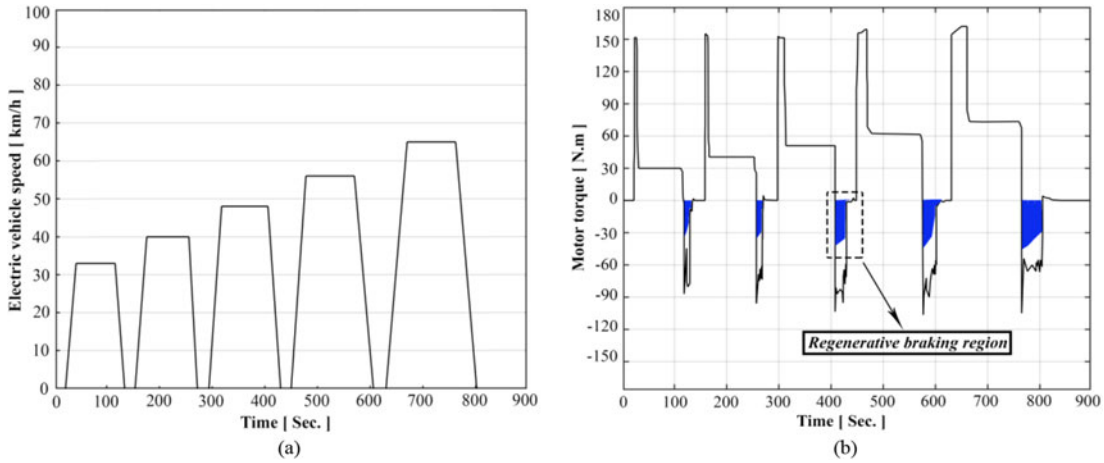

Fig. 14. Simulated speed and torque curves of the proposed regenerative braking system. (a) Simulated speed curve of WVU five-peak drive-cycle. (b) Motor–Generator torque curve of the proposed regenerative braking system.

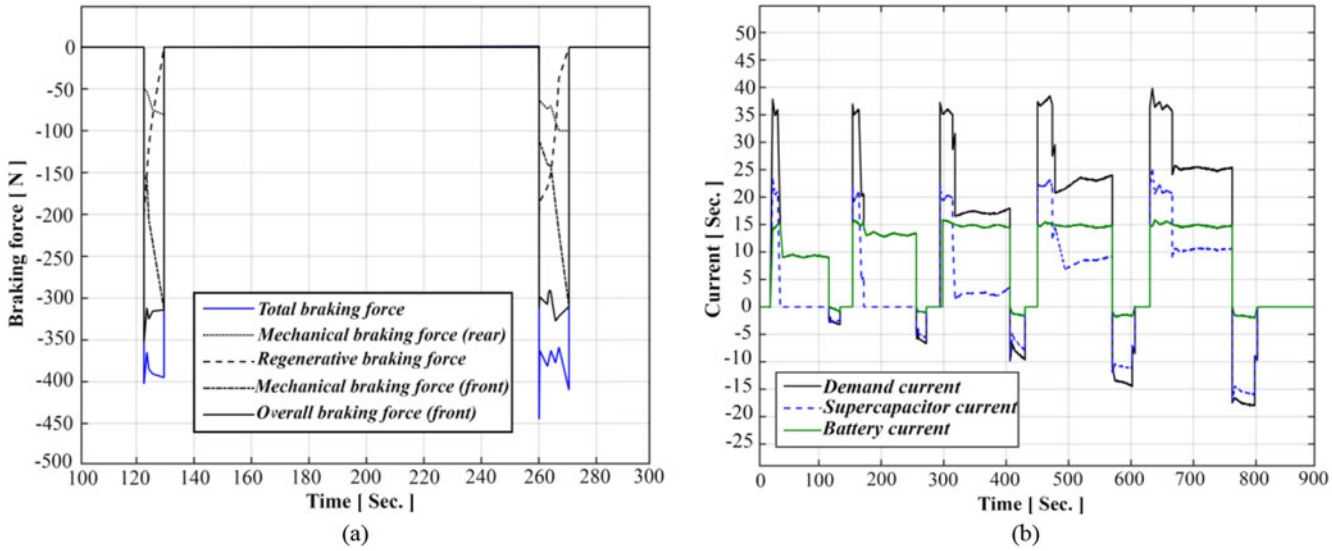

Fig. 15. Simulation results of the braking force distribution and current waveforms of battery, supercapacitor, and motor. (a) Braking force distribution on between the front and rear wheels of the EV. (b) Simulated current waveforms of the battery, supercapacitor, and motor.

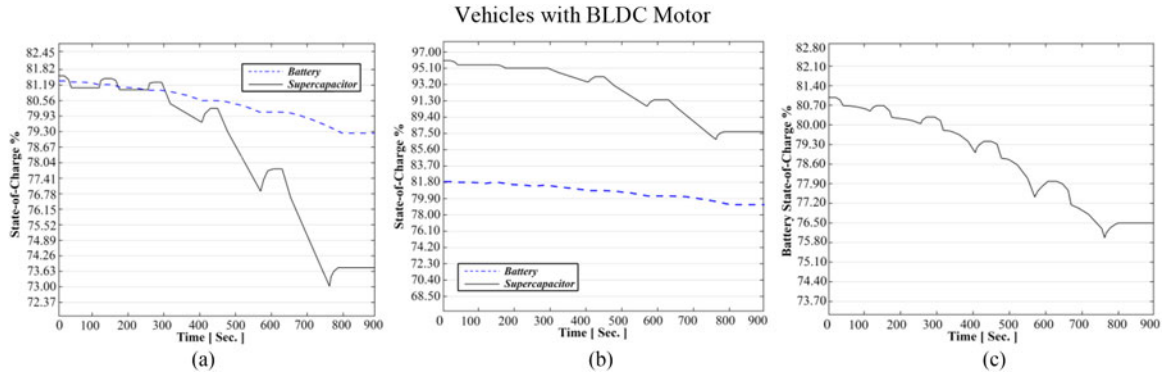

Fig. 16. SOCs of the battery and supercapacitor. (a) SOCs of the battery and supercapacitor when the initial SOCs are 81.3% and 81.8%, respectively. (b) SOCs of the battery and supercapacitor when the intial SOCs are 81.3% and 97%, respectively. (c) SOC of the battery in the EV without HESS when the initial SOC of the battery is 81.3%.

In Fig. 14(b), the motor–generator torque curve of the EV is depicted. During the EV acceleration, the required motor torque reaches about 150 N·m. The shaded area shows the regenerative braking region in which the energy is fed back to the HESS. At increased constant speeds, the regenerative braking torque is increased, which clearly demonstrates the efficient operation of the proposed ANN controller. It is generally difficult to achieve regenerative braking at low EV speed due to relatively low voltage generated by the motor/generator. If the mechanical braking is not engaged under such circumstances, the EV will not stop in the specified distance. Hence, it is seen that the ANN controller reduces the regenerative braking torque as the EV speed decreases, ensuring reliable operation of the braking system. Additionally, the braking force distribution between the rear wheel, front wheel, and division of the mechanical and regenerative forces are fulfilled real time by the ANN controller, as shown in Fig. 15(a). It can be concluded that the braking force of the rear wheel is considerably smaller than the braking force of the front wheel. Moreover, the portion of the regenerative braking is increased at higher constant speeds.

It is also seen that the portion of the regenerative braking will be significantly lowered by the ANN controller in low vehicle speeds, and more weight is allocated to frictional braking for secure deceleration of the EV.

During the EV acceleration, as seen in Fig. 14(b), a high transient torque is demanded by the electric motor. Hence, a very high transient current may be drawn from the energy storage unit, which can considerably lower the life time of the battery. As seen in Fig. 15(b), the supercapacitor assists the battery pack during the EV accelerations and EV high speeds. While the maximum discharge current of the battery is set to 15 A, the supercapacitor provides the rest of the demanded current through controlling the PWM in the DC/DC buck converter. Furthermore, it is observed that the high braking current is harvested by the supercapacitor bank, which not only increases the efficiency of the braking (due to lower ESR and very high power density) but also keeps the battery from high charge currents. If the supercapacitor cannot accept further charge from regenerative braking due to being fully charged, the proposed braking system will adjust the DC-link voltage for regenerative braking through the battery. Although the ANN will decrease the weight of the regenerative braking force under such conditions, the charging current of the battery will remain lower than the safe threshold (usually C-rate of the battery).

The efficiency of the method can be intuitively evaluated by comparing the SOC of the HESS during the drive-cycle. In the first case, the initial SOCs of the battery and supercapacitor are set to 81.3% and 81.8%, respectively. Therefore, since the voltage of the supercapacitor is far below the upper safety threshold (94%), the regenerative braking mode with battery could never be activated. Consequently, only the supercapacitor is utilized to absorb the braking energy. The SOCs of the battery and supercapacitor in this case are shown in Fig. 16(a). Fig. 16(b) shows the second case in which the initial SOC of the supercapacitor is set to 97%. Since the initial SOC of the supercapacitor is beyond the security margin at the first and second braking scenarios, the supercapacitor cannot absorb the braking energy, and hence, the regenerative braking with battery is activated. In the rest of the drive cycle, the supercapacitor discharges below the safety margin, and hence, the supercapacitor can be utilized for regenerative braking. In Fig. 16(c), the SOC of the battery is shown when the EV is driven only with the battery.

For the aforementioned two scenarios, where the SOCs of the supercapacitor are 81.8% and 97%, the efficiency is calculated as 48% and 43.5%, respectively. In the second case, since the supercapacitor initial voltage is beyond the safety margin during the first two braking scenarios, the battery is used for regenerative braking. Since the maximum charge current of the battery is limited, most of the braking energy will

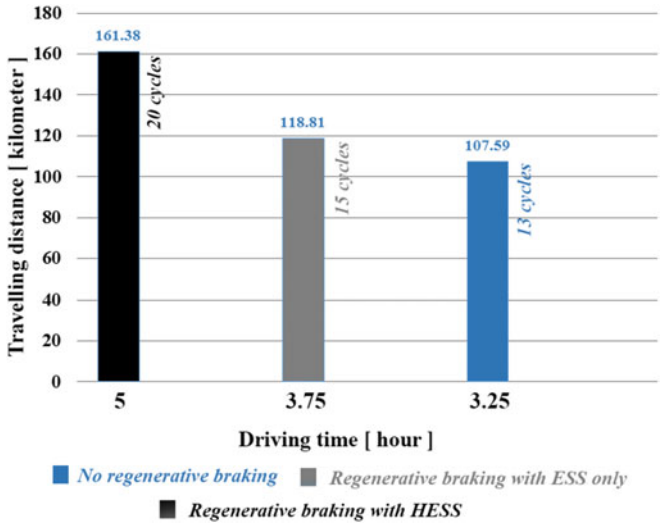

Fig. 17. Driving range of the simulated EV using WVU 5-peak driving pattern.

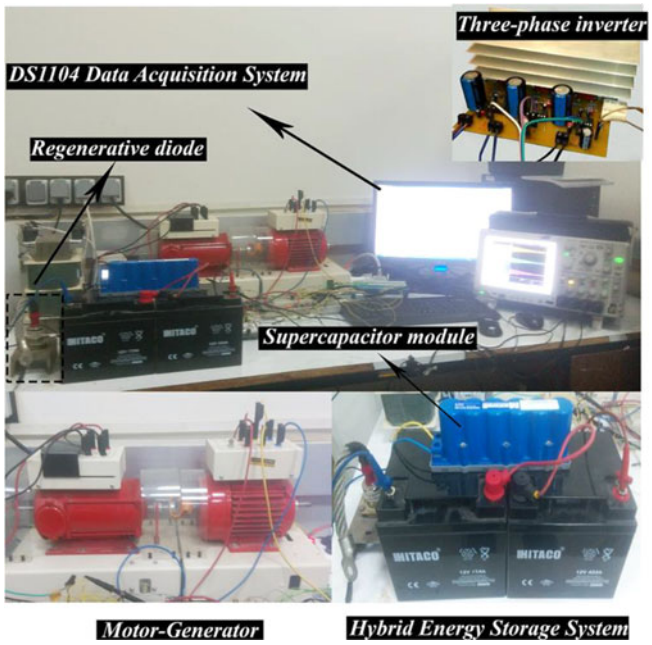

Fig. 18. Test bench of the proposed regenerative braking system.

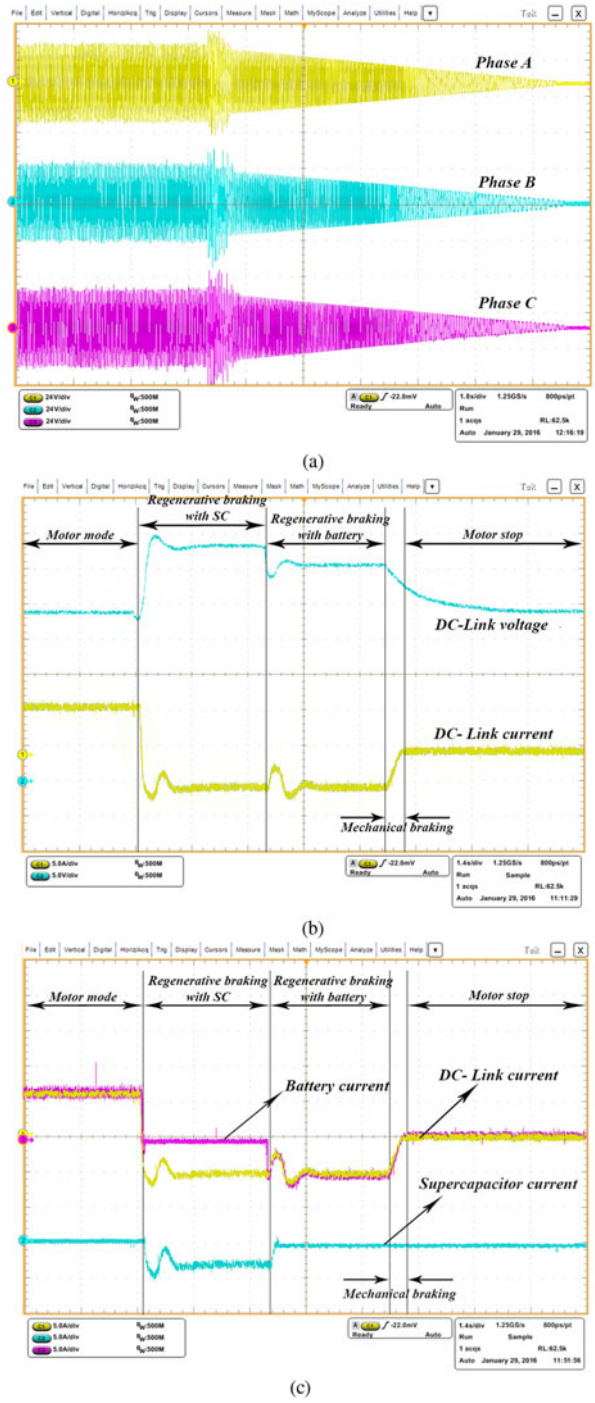

Fig. 19. Experimental results of the proposed RBS. (a) Three-phase back EMFs of the stator windings during normal conditions and regenerative braking. (b) Voltage and current waveforms of the dc-link during normal conditions and regenerative braking. (c) Experimental current waveforms of battery, supercapacitor, and dc-link during normal and regenerative modes.

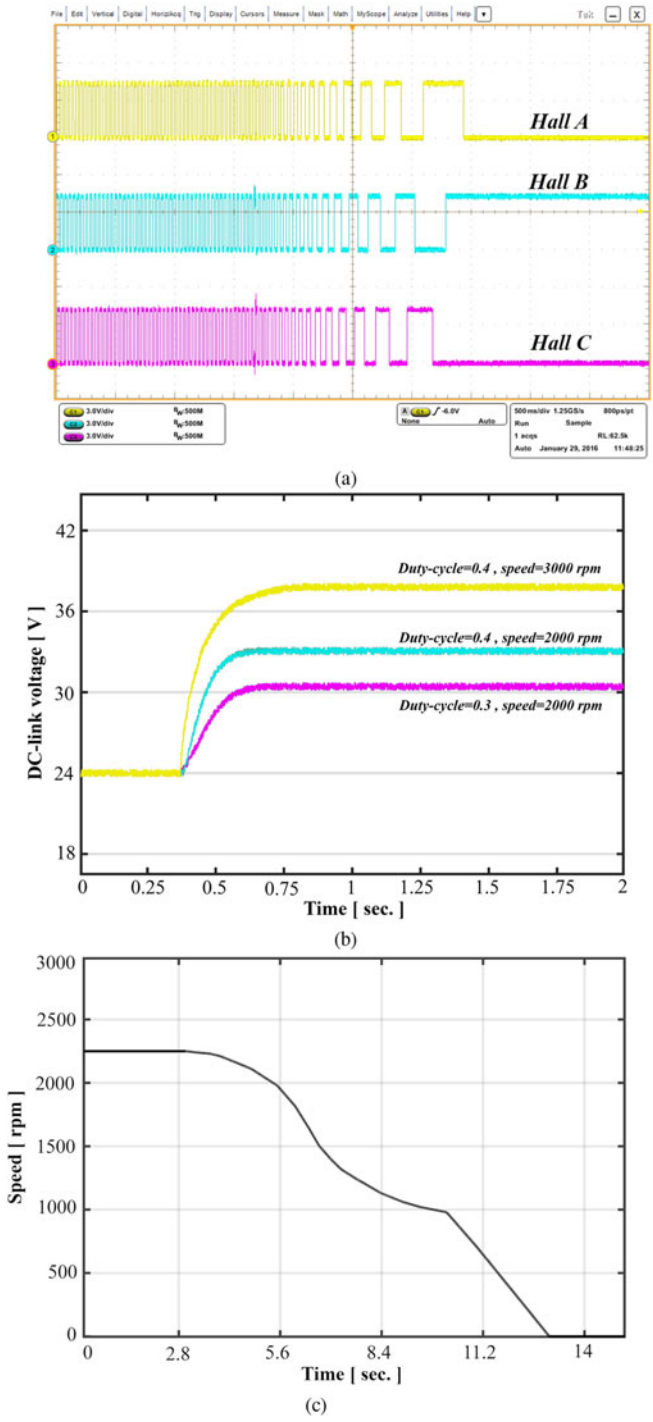

Fig. 20. Experimental results of the proposed RBS. (a) Voltage waveforms of the hall affect sensors when the BLDC motor is decelerating. (b) DC-link voltage at different duty-cycles and different speeds. (c) Speed of the BLDC motor in different modes, including normal mode, regenerative braking with supercapacitor, regenerative braking with battery, and mechanical braking.

be transferred to heat through the frictional braking. Therefore, according to (22), efficiency of the regenerative braking is decreased to 4.5%. In case of the EV driven only with the battery, the efficiency is decreased about 20% compared to case 1.

In (22), a large portion of the kinetic energy of the vehicle is wasted by the rear and front mechanical braking. Hence, the drive range of the vehicle is computed to evaluate the performance of the RBS more intuitively. It is assumed that the HESS is fully charged. Therefore, the initial SOCs of the battery and

the supercapacitor are chosen 98% and 96%, respectively, and the result is shown in Fig. 17.

When the pure mechanical braking is utilized and the EV uses ESS (battery), the drive range is approximately 13 cycles. Each cycle of the driving pattern shown in Fig. 14(a) represents a distance of about 8 km. Hence, it is shown that using HESS and the proposed RBS can increase the drive range of the EV by about 54 km. Likewise, the drive range is improved by about 43 km in comparison with the regenerative braking with ESS.

To evaluate the performance of the proposed RBS in real life, some experiments are carried out in the laboratory. Fig. 18 shows the laboratory test bench of the proposed regenerative braking scheme. The specifications of the test bench are tabulated in Table III.

For activation of both regenerative modes, the supercapacitor voltage is set near its maximum threshold. Waveforms of the back EMFs of the stator windings, the dc-link current, dc-link voltage, supercapacitor current, and battery current during braking state are shown in Fig. 19. When the brake command is applied, the controller first adjusts the dc-link voltage for constant torque braking with supercapacitor. During this time interval, the most of the dc-link current is harvested by the supercapacitor, and the battery current is relatively zero. When the supercapacitor voltage reaches the maximum safety threshold, the controller adjusts the dc-link voltage for constant torque braking with battery. Under these conditions, the dc-link voltage is lower than the supercapacitor voltage, and D_1 is reverse biased. Hence, the supercapacitor current is zero, and the whole dc-link current is charging the battery pack. Upon starting the braking procedure, the back EMFs of the generator start to decrease. When these three-phase back EMFs are too small, the controller switches to frictional braking. The status of the three-phase hall effect sensors during deceleration of the electric motor is shown in Fig. 20(a). In Fig. 20(b), the dc-link voltage at different duty-cycles and speeds is shown. It is evident that the proposed RBS with the switching algorithm discussed in Section III works properly. One can conclude that by adjusting the PWM duty-cycle in the inverter, the DC-link voltage can be varied. The waveform of the speed for the motor during decelerating is also shown in Fig. 20(c).

V. Conclusion

In this paper, a new RBS based on utilization of HESS is proposed for EVs driven by BLDC motor. During regenerative braking and/or energy regeneration, the kinetic energy of the vehicle is harvested by the supercapacitor using the appropriate switching template of the inverter. Hence, the need for additional power electronics interfaces is eliminated. Meanwhile, the MLP-ANN controller is utilized to control the braking force distribution between rear and front wheels of the EV. Moreover, the PI controller is used to control the duty-cycle of the PWM in the inverter to realize constant torque braking.

In comparison with other similar types of the regenerative braking schemes, the proposed method has the superiorities of being simple and high efficient. The EV is simulated in WVU 5-peak drive cycle, and it is shown that in comparison with the regenerative braking with ESS, the efficiency of the regeneration is improved by about 20%. Moreover, it is shown that the drive range of the EV is increased by about five cycles. It can be concluded that the presented scheme is able to capture the braking energy with appropriate efficiency and ensures the safe deceleration of the EV.

VI. Appendix

Data of the drive cycle used for training the ANN are shown in Table V.

TABLE V
Specifications of the Drive-Cycle Used for Training the ANN

Parameter	Value
Name	INRETS route1
Total distance	7814.57 m
Total time	888 s
% of time deaccelerating	42.79%
% of time cruising	6.19%
Average speed	31.7 km/h
Maximum speed	69.71 km/h
Average negative acceleration	-0.663 m/s^2

References

[1] A. Emadi, "Transportation 2.0," *IEEE Power Energy Mag.*, vol. 9, no. 4, pp. 18–29, Aug. 2011.

[2] A. Emadi, *Advanced Electric Drive Vehicles*. Boca Raton, FL, USA: CRC Press, Oct. 2014, ch. 8.

[3] Y. Kim and N. Chang, *Design and Management of Energy-Efficient Hybrid Electric Energy Storage Systems*. Hoboken, NJ, USA: Springer, 2014, pp. 19–25.

[4] A. Khaligh and Z. Li, "Battery, ultracapacitor, fuel cell, and hybrid energy storage systems for electric, hybrid electric, fuel cell, and plug-in hybrid electric vehicles: State of the art," *IEEE Trans. Veh. Technol.*, vol. 59, no. 6, pp. 2806–2814, Apr. 2010.

[5] S. Kim and S. H. Choi, "Development of fuel cell hybrid vehicle by using ultra-capacitors as a secondary power source," in *Proc. SAE World Congr.*, Detroit, MI, USA, Apr. 2005.

[6] M. Ortuzar, J. Moreno, and J. Dixon, "Ultracapacitor-based auxiliary energy system for an electric vehicle: Implementation and evaluation," *IEEE Trans. Ind. Electron.*, vol. 54, no. 4, pp. 2147–2156, Aug. 2007.

[7] L. Gao, R. A. Dougal, and S. Liu, "Power enhancement of an actively controlled battery/ultracapacitor hybrid," *IEEE Trans. Power Electron.*, vol. 20, no. 1, pp. 236–243, Jan. 2005.

[8] W. Lhomme, P. Delarue, P. Barrade, A. Buoscayrol, and A. Rufer, "Design and control of a supercapacitor storage system for traction applications," in *Proc. IEEE Ind. Appl. Conf.*, Kowloon, Hong Kong, Oct. 2005, pp. 2013–2020.

[9] Z. Jiang and R. A. Dougal, "A compact digitally controlled fuel cell/battery hybrid power source," *IEEE Trans. Ind. Electron.*, vol. 53, no. 4, pp. 1094–1104, Jun. 2006.

[10] S. M. Lukic, S. G. Wirashanga, F. Rodriugez, C. Jian, and A. Emadi, "Power management of an ultracapacitor/battery hybrid energy storage system in an HEV," in *Proc. IEEE Veh. Power Propulsion Conf.*, Windsor, U.K., 2006, pp. 1–6.

[11] L. Solero, A. Lidozzi, and J. A. Pomilio, "Design of multiple-input power converter for hybrid vehicles," *IEEE Trans. Power Electron.*, vol. 20, no. 5, pp. 1007–1016, Sep. 2005.

[12] S. M. Lukic, J. Cao, R. C. Bansal, F. Rodriguez, and A. Emadi, "Energy storage systems for automotive applications," *IEEE Trans. Ind. Electron.*, vol. 55, no. 6, pp. 2258–2267, Jun. 2008.

[13] Z. Li, O. Onar, A. Khaligh, and E. Schaltz, "Power management, design, and simulations of a battery/ultracapacitor hybrid system for small electric vehicles," in *Proc. SAE World Congress*, Detroit, MI, USA, Apr. 2009.

[14] H. Matsuo, L. Wenzhong, F. Kurokawa, T. Shigemizu, and N. Watanabe, "Characterization of the multiple-input DC–DC converter," *IEEE Trans. Ind. Electron.*, vol. 51, no. 3, pp. 625–631, Jun. 2004.
[15] M. Marchesoni and C. Vacca, "New DC–DC converter for energy storage system interfacing in fuel cell hybrid electric vehicles," *IEEE Trans. Power Electron.*, vol. 22, no. 1, pp. 301–308, Jan. 2007.
[16] M. C. Kisacikoglu, M. Uzunoglu, and M. S. Alam, "Fuzzy logic control of a fuel cell/battery/ultra-capacitor hybrid vehicular power system," in *Proc. Veh. Power Propulsion Conf.*, Arlington, TX, USA, 2007, pp. 591–596.
[17] B. G. Dobbs and P. L. Chapman, "A multiple-input DC–DC converter topology," *IEEE Power Electron. Lett.*, vol. 1, no. 1, pp. 6–9, Mar. 2003.
[18] H. J. Chiu, H. M. Huang, L. W. Lin, and M. H. Tseng, "A multiple-input DC/DC converter for renewable energy systems," in *Proc. IEEE Conf. Ind. Technol.,* Hong Kong, 2005, pp. 1304–1308.
[19] Y. M. Chen, Y. C. Liu, and F. Y. Wu, "Multi-input DC/DC converter with ripple-free input currents," in *Proc. IEEE Power Electron. Spec. Conf.*, Australia, 2002, pp. 796–802.
[20] Z. Li, O. Onar, A. Khaligh, and E. Schaltz, "Design and control of a multiple input DC/DC converter for battery/ultracapacitor based electric vehicle power system," in *Proc. IEEE Conf. Appl. Power Electron. Expo.*, Washington, DC, USA, Feb. 2009, pp. 591–596.
[21] J. Cao and A. Emadi, "A new battery/ultracapacitor hybrid energy storage system for electric, hybrid, and plug-in hybrid electric vehicles," *IEEE Trans. Power Electron.*, vol. 27, no. 1, pp. 122–132, May 2011.
[22] J. M. Blanes, R. Gutierrez, A. Garrigós, J. L. Lizán, and J. M. Cuadrado, "Electric vehicle battery life extension using ultracapacitors and an FPGA controlled interleaved buck–boost converter," *IEEE Trans. Power Electron.*, vol. 28, no. 12, pp. 5940–5948, Mar. 2013.
[23] M. E. Choi, S. W. Kim, and S. W. Seo, "Energy management optimization in a battery/supercapacitor hybrid energy storage system," *IEEE Trans. Smart Grid*, vol. 3, no. 1, pp. 463–472, Oct. 2011.
[24] S. G. Wirasingha and A. Emadi, "Classification and review of control strategies for plug-in hybrid electric vehicles," *IEEE Trans. Veh. Technol.*, vol. 60, no. 1, pp. 111–122, Oct. 2010.
[25] O. Hegazy, J. Van-Mierlo, and P. Lataire, "Analysis, modeling, and implementation of a multidevice interleaved DC/DC converter for fuel cell hybrid electric vehicles," *IEEE Trans. Power Electron.*, vol. 27, no. 11, pp. 4445–4458, Jan. 2012.
[26] X. Nian, F. Peng, and H. Zhang, "Regenerative braking system of electric vehicle driven by brushless DC motor," *IEEE Trans. Ind. Electron.*, vol. 61, no. 10, pp. 5798–5808, Jan. 2014.
[27] N. Mutoh, "Driving and braking torque distribution methods for front- and rear-wheel-independent drive-type electric vehicles on roads with low friction coefficient," *IEEE Trans. Ind. Electron.*, vol. 59, no. 10, pp. 3919–3933, Feb. 2012.
[28] M. Montazeri and M. Soleymani, "Investigation of the energy regeneration of active suspension system in hybrid electric vehicles," *IEEE Trans. Ind. Electron.*, vol. 57, no. 3, pp. 918–925, Oct. 2009.
[29] S. M. Yang and J. Y. Chen, "Controlled dynamic braking for switched reluctance motor drives with a rectifier front end," *IEEE Trans. Ind. Electron.*, vol. 60, no. 11, pp. 4913–4919, Dec. 2012.
[30] L. Wang, E. G. Collins, and H. Li, "Optimal design and real-time control for energy management in electric vehicles," *IEEE Trans. Veh. Technol.*, vol. 60, no. 4, pp. 1419–1429, Mar. 2011.
[31] H. J. Chiu and L. W. Lin, "A bidirectional DC-DC converter for fuel cell electric vehicle driving system," *IEEE Trans. Power Electron.*, vol. 21, no. 4, pp. 950–958, Jul. 2006.
[32] D. A. Bender, "Method and apparatus for power electronics and control of plug-in hybrid propulsion with fast energy storage," U.S. Patent 7 740 092, Jun. 22, 2010.
[33] J. Ko *et al.*, "Development of brake system and regenerative braking cooperative control algorithm for automatic-transmission-based hybrid electric vehicles," *IEEE Trans. Veh. Technol.*, vol. 64, no. 2, pp. 431–440, May 2014.
[34] S. Lu, P. Weston, S. Hillmansen, H. B. Gooi, and C. Roberts, "Increasing the regenerative braking energy for railway vehicles," *IEEE Trans. Intell. Transp. Syst.*, vol. 15, no. 6, pp. 2506–2515, May 2014.
[35] A. Fazeli, M. Zeinali, and A. Khajepour, "Application of adaptive sliding mode control for regenerative braking torque control," *IEEE/ASME Trans. Mechatronics*, vol. 17, no. 4, pp. 745–755, Apr. 2011.
[36] S. de la Torre, A. J. Sánchez-Racero, J. A. Aguado, M. Reyes, and O. Martianez, "Optimal sizing of energy storage for regenerative braking in electric railway systems," *IEEE Trans. Power Syst.*, vol. 30, no. 3, pp. 1492–1500, Aug. 2014.
[37] M. Mortazavi, M. Mastali, and A. A. Safavi, "Enhanced neural network based fault detection of a VVER nuclear power plant with the aid of principal component analysis," *IEEE Trans. Nucl. Sci.*, vol. 55, no. 6, pp. 3611–3619, Dec. 2008.
[38] G. Hongwei, G. Yimin, and M. Ehsani, "A neural network based SRM drive control strategy for regenerative braking in EV and HEV," in *Proc. Elect. Mach. Drives Conf.*, Jun. 2001, pp. 571–575.

Farshid Naseri (S'16) received the B.Sc. degree in electrical engineering from Shiraz University of Technology, Shiraz, Iran, in 2013, and the M.Sc. degree in electrical power engineering from Shiraz University, Shiraz, in 2015, where he is currently working toward the Ph.D. degree in electrical power engineering. His research interests include power electronics, electric vehicle systems, and intelligent control.

Ebrahim Farjah (M'12) received the B.Sc. degree in electrical and electronics engineering from Shiraz University, Shiraz, Iran, in 1987, the M.Sc. degree in electrical power engineering from Sharif University of Technology, Tehran, Iran, in 1989, and the Ph.D. degree in electrical engineering from Grenoble Institute of Technology, Grenoble, France, in 1994.

He is currently a Professor in the Department of Electrical and Computer Engineering, Shiraz University. His research interests include power electronics, renewable energy, micro-grids, and power quality.

Teymoor Ghanbari received the B.Sc. degree in electrical power engineering from S.R. University, Tehran, Iran, in 1996, the M.Sc. degree in electrical power engineering from Shahrood University of Technology, Shahrood, Iran, in 2006, and the Ph.D. degree in the same field from Shiraz University, Shiraz, Iran, in 2012.

He is currently an Assistant Professor in the School of Advanced Technologies, Shiraz University. His research interests include distributed generation, power electronics, and electrical machines.